Dielectric, Energy Storage, and Loss Study of Antiferroelectric-Like Al-doped HfO_2 Thin Films

Alexis Payne[1,2,a)], Owen Brewer[3], Asher Leff[1], Nicholas A. Strnad[1], Jacob L. Jones[2], Brendan Hanrahan[1]
[1]Sensors and Electron Devices Directorate, US CCDC Army Research Laboratory, Adelphi, Maryland, 20783, USA
[2]Materials Science and Engineering Department, North Carolina State University, Raleigh, North Carolina, 27606, USA
a) Author to whom correspondence should be addressed: alpayne2@ncsu.edu

Abstract:

Antiferroelectric thin films have properties ideal for energy storage due to their lower losses compared to their ferroelectric counterparts as well as their robust endurance properties. We fabricated Al-doped HfO_2 antiferroelectric thin films via atomic layer deposition at variable thicknesses (20nm or 50nm) with varying dopant concentration (4 at% or 8 at%). 50nm thick 8 at% Al-doped HfO_2 showed a maximum energy storage density of 63 J/cm^3 while maintaining an efficiency of 85%. A study comparing these thin films revealed thicker films allowed for higher operating electric fields and thus higher energy storage densities at operating voltage. The loss tangents of the thin films at operating voltage were under 2% over the range of -4 to 4 MV/cm and at frequencies ranging from 500Hz-100 kHz. Reliability studies showed the thin films endure up to 10^6-10^7 cycles and the breakdown field of the films yielded Weibull moduli greater than 6 for all our thin films. The Weibull modulus provides a measurement of the consistency of the breakdown strength from sample to sample, with a higher moduli indicating a more invariable result. These electrical characteristics along with the thin film's cycling endurance and reliability make antiferroelectric-like Al-doped thin films a promising material for energy storage applications.

Antiferroelectric thin films have the potential to play a role in many electronic devices due to their large energy storage densities capable of producing ultrahigh currents at small scale. Recent advances in the production of ferroelectric (FE) and antiferroelectric (AFE) thin films grown via atomic layer deposition (ALD) have enabled device miniaturization in applications like non-volatile memory (FRAM) and energy storage devices.[1,2] The most common AFE materials are lead-based, such as $PbZrO_3$. These materials are known to have large energy storage densities (~25 J/cm^3) [3–5] but have environmental and health issues which restrict their use in certain countries (e.g. European Union Restriction on Hazardous Substances (ROHS)). Hafnia-based FEs and AFEs are gaining prominence as a viable alternative to their lead-based counterparts. Energy storage density (ESD) values are regularly assessed for AFE and AFE-like, FE, and dielectric (DE) thin films. The reason for the "AFE-like" nomenclature in this work is the current lack of consensus of the physical origins of the hysteresis "double loop" characteristic of AFEs.[6–10] The most prevalent theory behind the AFE behavior is the zero remanent polarization is caused by a reversible field induced phase transition from tetragonal to orthorhombic phase.[6] The orthorhombic phase, *Pca*2$_1$, is the ferroelectric phase for Hf-based thin films while the tetragonal phase, *P*4$_2$*/nmc*, is not ferroelectric.[7,8] Another theory for the double hysteresis/AFE-like response of Hf-based thin films is there might be a different polar phase.[11] It has also been suggested that there is no reason the *Pca*2$_1$ could not exist in an antipolar state, with ferroelectric domains oriented in antiparallel.[7] There has also been evidence to suggest that interfacial charged defects act as pinning sites for domain wall motion inhibiting the total switchable polarization of the thin film.[6,9,10] In terms of ESD, the low or zero remanent polarization observed in these films, regardless of physical origin, is

beneficial. Energy is stored when either the material is transitioning from FE to AFE or pinning caused by charged defects is overcome.

The polarization versus electric field data of a thin film can be integrated via equations 1 and 2 to calculate the ESD of the thin film.[12,13]

$$W_{tot} = \int_0^{P_{max}} EdP \quad \text{Eq. 1}$$

$$W_{rec} = \int_{P_{max}}^{-P_r} EdP \quad \text{Eq. 2}$$

Where W_{tot} is total energy density, W_{rec} is recoverable energy density also known as the ESD, E is the applied electric field , P_{max} is the maximum polarization, and P_r is the remanent polarization. The energy loss (W_{loss}) can be calculated from W_{tot}- W_{rec} . From equations 1 and 2 it can be seen that higher differences in maximum and remanent polarization yield higher efficiency storage, guiding materials selection toward AFEs. The efficiency, η, is defined as follows. [12,13]

$$\eta = \frac{W_{rec}}{W_{tot}} \times 100\% = \frac{W_{rec}}{W_{rec}+W_{loss}} \times 100\% \quad \text{Eq. 3}$$

Thus, in terms of energy storage capabilities, AFE/AFE-like materials have significant advantages over both linear dielectrics and ferroelectrics due to their remanent polarization being zero, or almost zero and their ability to become highly polarized at high fields. Relaxor ferroelectric thin films have been studied for energy storage as well, for example $Ba(Zr,Ti)O_3/(Ba,Ca)TiO_3$ thin films have been studied reporting ESD values of 42.1 J/cm^3 at 43% efficiency[14], another relaxor ferroelectric $(Bi,Na)BaTiO_3/BiFeO_3$ had reported values of 31.96 J/cm^3 with 61% efficiency.[15] Recently, PMN-PT thin film reported an ESD value of 133 J/cm^3 at 75% efficiency, but that required a costly heavy ion bombardment sample treatment.[16] Comparatively, AFE/AFE-like HfO_2 materials have had reported ESDs of 61.2 J/cm^3 with 65% efficiency ($Si:HfO_2$)[17], 45 J/cm^3 with 50% efficiency ($Hf_{0.3}Zr_{0.7}O_2$)[18], 52 J/cm^3 with 80% efficiency ($Al:Hf_{0.5}Zr_{0.5}O_2$)[19], 54 J/cm^3 with 82% efficiency ($Si:Hf_{0.5}Zr_{0.5}O_2$).[19] AFE/AFE-like HfO_2 based thin films show superior ESDs with higher efficiencies than that of many relaxor ferroelectric thin films.

HfO_2 based thin films have been shown to have the ability to endure 10^9 cycles at 75% to as high as 90% of their breakdown field (E_{BD})[17–19]. It has been noted that the endurance properties of AFEs are typically greater than that of their FE counter parts.[20–24]A possible explanation for why this is comes from the strain induced by the change in polarization from a 180° reorientation (AFE) is less than that induced by a 90° reorientation (FE).[24] Models have suggested the reason for the reduced fatigue in AFE materials compared to FE materials is due to the charge injection during switching at the electrode interfaces.[20] A lower charge injection is required in AFEs versus FEs due to the depolarization field near the electrode being significantly less in AFEs than FEs.[20] These same trends have been seen in Si-doped HfO_2 thin films, with FE Si-doped thin films experiencing a wake-up period and significant fatigue after 10^8 cycles while the AFE Si-doped HfO_2 thin films experienced no wake-up period and had not fatigued after 10^8 cycles.[25]

The breakdown field strength, E_{BD}, is generally higher for ALD-deposited HfO_2 (> 5 MV/cm) compared with other ferroelectric materials, such as $Pb(Zr,Ti)O_3$ and $BaTiO_3$ which breakdown typically < 1 MV/cm. The value for undoped HfO_2 at the nanometer scale has been reported as high as 13000 kV/cm.[26] For ferroelectric HfO_2, $Si:HfO_2$ applied to a 3D structured substrate was shown to have a breakdown field as high as 4200 kV/cm.[27] However, there exists a fundamental trade-off between E_{BD} and the dielectric constant, ε_r, of a material, as materials with high E_{BD} typically have low dielectric constants.[28] Thus, the dielectric constants of the HfO_2 based thin films is not as great as those seen in $Pb(Zr,Ti)O_3$ thin films ($\varepsilon_r \approx$ 850-1200)[29] or $BaTiO_3$ thin films ($\varepsilon_r \approx$300-3200)[30,31]. The dielectric constant of $HfO_{0.3}Zr_{0.7}O_2$ has been reported as 30-45 based on applied field and thin film thickness.[18] Si-doped HfO_2 has also had reported values ranging from 21-46 for dielectric constant at various dopant concentrations.[32] In terms of ESD, it can be beneficial to have both a large ε_r and E_{BD}, however, in terms of devices, a larger breakdown field is often more critical as it enables the device to be used in a wider range of applications. The operating voltage (V_{op}) for commercial capacitors

is normally 4-5 times below that of the breakdown voltage (V_{BD}) of the device. For multilayer ceramic capacitors it has been shown the rated voltage was 10 times below the V_{BD},[33] and tantalum capacitors have been tested up to 132% of their rated voltage.[34] Thus, in terms of commercial devices, HfO_2 based thin film's larger breakdown fields would be beneficial.

Understanding how HfO_2 based thin films operate at different temperatures and frequencies is also critical to device development. FE Si:HfO_2 capacitance vs. voltage measurements were recorded between 298 K and 438 K, revealing ~28% jump in capacitance over that range.[35] ESD values have been recorded as a function of temperature for Si:HfO_2, increasing 28% between 210 K and 400 K.[17] ESD values were also shown to be stable up to 400K for $Hf_{0.3}Zr_{0.7}O_3$[18] , Si:$Hf_{0.5}Zr_{0.5}O_3$[19], and Al:$Hf_{0.5}Zr_{0.5}O_3$.[19] However, there has been virtually no studies on the effect of frequency on dielectric properties or losses of HfO_2 based thin films. A single study to date shows the impedance of Gd:HfO_2 was shown to decrease by 3 orders of magnitude over 1 Hz- 1 MHz.[36]

The AFE-like thin films were grown on a Si substrate with 500 nm of thermally-grown SiO_2 followed by a sputtered Ti layer which was then oxidized, the 32nm TiO_2 layer serves as an adhesion layer for Pt. The Pt-bottom electrode was then sputtered onto the Si/SiO_2/TiO_2 substrate via DC magnetron sputtering to a nominal thickness of 100 nm. The thin films were grown via ALD. The precursors used were tetrakis dimethylamino hafnium (TDMAH) and trimethylaluminum (TMA) with H_2O as the oxygen precursor. The inert purge gas was Ar. The substrate temperature during growth was held at 250 °C. The composition of the film was varied by changing the ratio of HfO_2 cycles to Al_2O_3 cycles ranging from 24:1 for 4 at% to 23:2 for 8 at%. The total number of cycles defined the film thickness. The thickness was measured using ellipsometry post growth, as well as checked via scanning electron microscopy (SEM).

The films were grown using a deposition, anneal, deposition, anneal (DADA) process. ALD growth began with an initial deposition ranging from 1-2 nm thick. The substrate was then removed from the ALD chamber and exposed to a rapid thermal anneal (RTA) at 300 °C for 60 seconds in N_2. This process was found to improve reliability which could be due to the removal of volatile organics at the Pt/Hf interface. Growth was then continued on the annealed sample. Once the film finished growth, the thickness was confirmed with ex-situ ellipsometry and matched the expected thicknesses, 20nm or 50nm, based on the standard growth rates of Al_2O_3 and HfO_2. After this ex-situ photolithography was used to define a top electrode pattern onto the substrate. The Pt top electrodes were sputtered ex-situ using DC magnetron sputtering at a nominal 100 nm thick. After top electrodes were placed, the samples underwent RTAs at temperatures ranging from 300 °C-900 °C. Annealing conditions of 700 °C for 60 seconds in N_2 were found to provide the best energy storage properties, the subsequent measurements and analysis were conducted on the 700 °C annealed thin films.

Grazing incidence X-ray Diffraction (GIXRD) data were taken for each 700°C annealed thin film sample using a Panalytical XRD system. For the GIXRD, the incident angle was set at 2.0°, with the data collected over a range 10°-90° for 2θ. AFE-like behavior in Si or Al doped $Hf_{0.5}Zr_{0.5}O_3$ has been attributed to an electric field induced phase transition between the non-polar tetragonal phase ($P4_2/nmc$) and the polar orthorhombic phase ($Pca2_1$).[19] Comparing the GIXRD spectra from various dopants and thicknesses, differences can be seen in the region of 28°-33° (Fig. 1b). The peak with highest intensity in the $Pca2_1$ orthorhombic phase is the 111 peak near 30°, which all samples show. This also could be the 101 peak of the tetragonal phase or a combination thereof. Distinguishing between these two phases is non-trivial without a high resolution measurement, either via x-ray or another technique. However, the 4 at% Al:HfO_2 thin film samples have two other peaks, at ~ 29° and ~ 32°, which correspond to the monoclinic $\bar{1}11$ and 111. The GIXRD clearly shows the 4 at% Al: HfO_2 thin films to contain some monoclinic phase present, which is not present in the 8 at% Al:HfO_2 thin films.

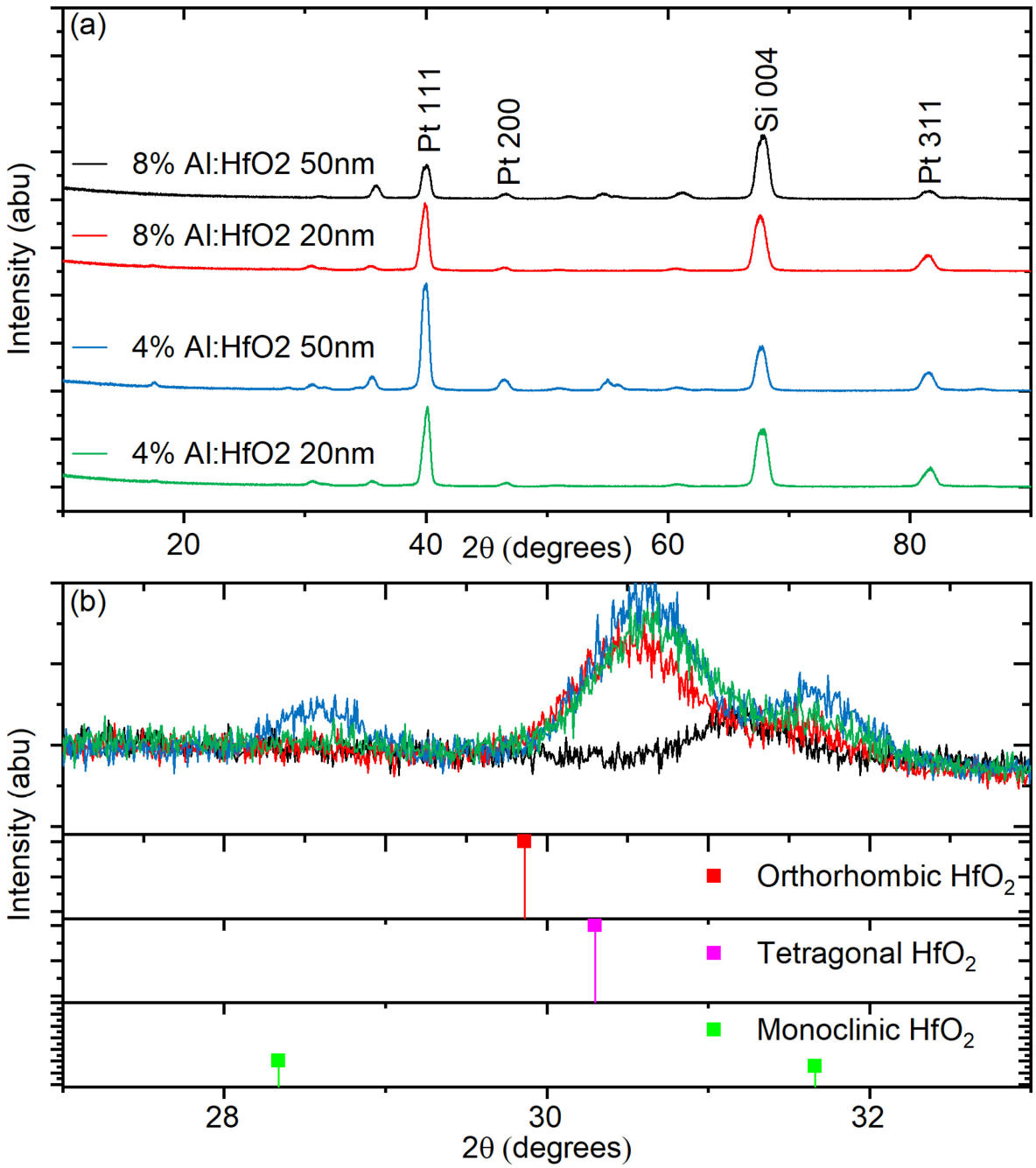

Figure 1: (a) GIXRD of all four Al:HfO_2 compositions, (b) around largest intensity orthorhombic/tetragonal peak and monoclinic peaks between 27-33.

Electrical characterization of the capacitors was performed using a *Radiant Technologies Precision Premier II*. Figure 3a shows the pristine polarization electric field (PE) loops for the sample set. The maximum electric field applied was 75% of breakdown (0.75E_{BD}) at a rate of 2 kHz. Thus, for the 4 at% Al:HfO_2 films voltages of 4 V and 10.8 V were applied to the 20nm thin film and 50nm thin film respectively. The 8 at% Al:HfO_2 20nm thin films had 4.4 V applied, and the 8 at% 50nm thin films had 14 V applied. Each ESD was calculated from a series of monopolar PE loops (Figure S1), each loop was taken at sequentially increasing fields until the device experienced breakdown. A monopolar loop was used instead of the typical bipolar loop as it is more relevant to high output power applications such as pulsed power technology.

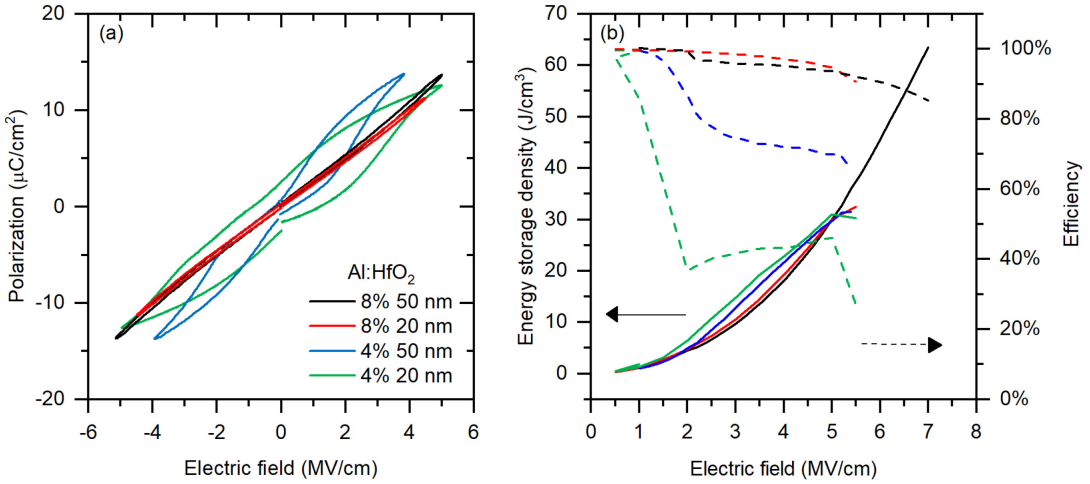

Figure 2: (a) Polarization versus electric field loops of thin film Al:HfO_2 of various compositions and thicknesses at 75%E_{BD} and (b) ESD and η calculations with increasing applied field.

The shape of the loop plays a significant role in the ESD and η values of the thin films. The 8 at % Al:HfO_2 PE loops shown in Figure 2a reach similar maximum polarization values as the 4 at% Al:HfO_2 loops while staying slimmer than the 4 at% Al:HfO_2 loops at those high fields. This leads to an increase in both ESD and efficiency for the slimmer loop 8 at% Al:HfO_2 samples compared to their 4 at% Al doped counterparts. With the 4 at% Al:HfO_2 20nm thin films, the efficiency dips and then rises again due the maximum polarization increasing faster than remanent polarization in the range of 2-5MV/cm (Figure S1). Unexpectedly, an increase in thickness yielded higher breakdown fields for both compositions, resulting in higher ESD potential. This is likely due to a reduction in electrode to electrode grain boundaries, as the 20nm thin films could be nominally 1 grain thick,[36] while the 50nm samples have more grains resulting in less through thickness grain boundaries.

The relative importance of η versus ESD should be re-evaluated when considering the application perspective. The energy lost in the system will dissipate as heat, which could pose as a challenge for many applications. Consider the record high energy density of 450 μJ/cm^2 obtained by Kühnel et al. for an area-enhanced AFE Si:HfO_2 film was 67% efficient.[37] Supposing the capacitor is used in a pulsed power application and is providing power pulses at 10kHz, it will have to dissipate ~15 W/cm^2 at minimum which means device-level energy density will be reduced by some volume dedicated to thermal management. For capacitors which are heat-sinked to a Si substrate this cooling requirement is not an issue, but in a device where the energy storage material makes up a sizeable fraction of the total volume, thermal changes will arise. Thermal requirements will scale linearly with frequency which could go to MHz levels for radio applications. The 8 at% Al:HfO_2 compositions have lower energy storage densities at a given voltage, but the extremely slim, efficient hysteresis loops could prove to be higher performance from an application perspective.

Figure 4 describes the dielectric breakdown distribution within the tested sample set. The Weibull modulus (β) refers to the reliability of the devices.[38] The Weibull distribution is calculated as follows, with $X_i = \ln(E_i)$ and $Y_i = \ln\left[\ln\left(1 - \frac{i}{n+1}\right)\right]$, where i is an individual sample, n is the total number of samples, and E_i is the breakdown strength of an individual sample. At least 10 data points were taken for each film. The Weibull modulus (β), is the slope of linear-fitted curves in the Weibull distribution and refers to the reliability of the devices.[38] The higher β is the more narrow the distribution of breakdown strengths for a set of samples, high moduli are desired as this indicates that samples are more predictable and less likely to breakdown at lower voltages. The higher β values calculated in Figure 3 show that 4 at% Al-doped HfO_2 samples have a narrower distribution of breakdown strengths than that of the 8 at% Al-doped HfO_2 samples, with moduli of 9.8 and 16.9 vs. 8.1 and 6.7.

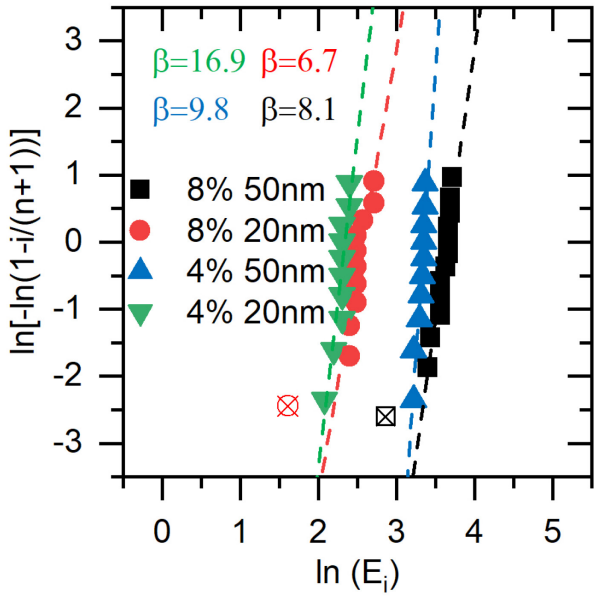

Figure 3: Weibull distribution of breakdown field for each Al:HfO_2 sample with the Weibull modulus listed for each one. The x'd data points were excluded from calculations as they suffered from early "infant mortality" failure.

Full, cross wafer analysis would be needed to fully establish the reliability of the breakdown strength for the various compositions.

An operating voltage is assumed for each sample based on the general rule of thumb where $V_{op} \sim 0.25*E_{BD}$. The ESD and η for the V_{op} are shown in table 1. The breakdown voltage (V_{BD}) for the thin films are listed as well. Comparing these thin films at theoretical operating voltages shows that their energy storage efficiencies would all be above 89%. The higher V_{BD} of the 8 at% Al:HfO_2 results in it having the highest theoretical V_{op} and subsequently the highest ESD values at operating voltage while still maintaining a higher η than either 4 at% Al-doped samples at V_{op}. Subsequent characterizations are performed above the estimated V_{op} showing the reliability of these devices even at higher levels.

Table 1 Electric characteristics for Al:HfO_2 Capacitors

Sample	V_{BD} [V]	V_{op} [V]	ESD @V_{op}[J cm^{-3}]	η @ V_{op}
4% Al:HfO_2 20nm	10	2	1.306	89%
4% Al:HfO_2 50nm	27	6	1.419	99%
8% Al:HfO_2 20nm	11	2	1.166	100%
8% Al:HfO_2 50nm	35	8	2.865	100%

The thin films underwent endurance cycling at 10kHz at 40%E_{BD} and no wake-up effect was observed up to 10^7 cycles for the 4 at% 50nm Al:HfO_2 and the 8 at% Al:HfO_2 samples. The remanent polarization (P_r) as well as P_{max} should little to no change with cycling with a triangular waveform as seen in Figure 4. However, the 4 at% 20nm Al:HfO_2 sample had a significantly higher P_r upon initial measurement, which continued to increase with cycling, it also only endured 10^6 cycles at 10kHz at 40%E_{BD}.

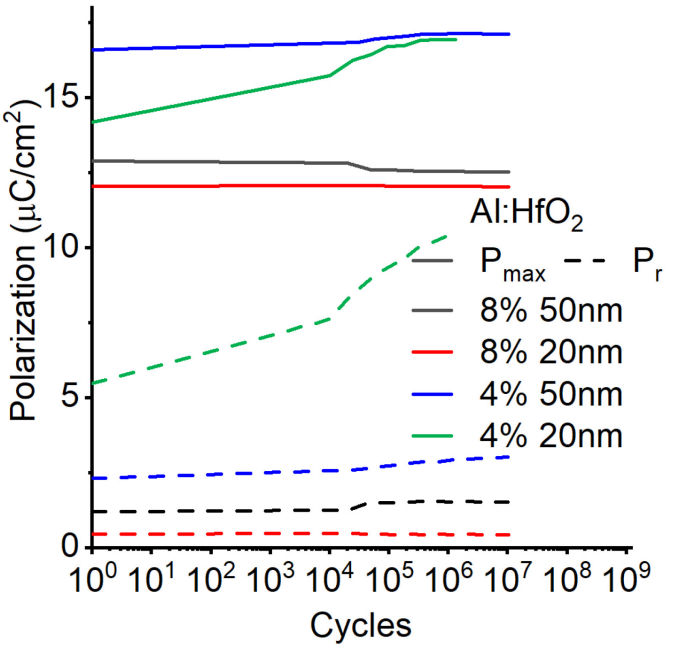

Figure 4: The endurance of the Al:HfO_2 films cycled at 40% of E_{BD} up to 10^6-10^7 cycles with a triangular waveform. How the P_r (dashed) and P_{max}(solid) change over this range of cycling is shown.

Permittivity and loss tangent were measured with bias and frequency using a small AC signal set up using a Keysight/Agilent 4192A LF Impedance Analyzer. The bias dependence in Figure 5a shows the loss tangent remains below 2% for all samples under varying field. A positive slope of $d\varepsilon_r/dE$ can be observed for both 8 at% Al-doping samples, with the 50nm showing a double loop, confirming AFE-like behavior. Figure 5B shows the frequency dependence ranging from 100Hz to 100kHz revealing flat permittivity and low loss through the range of tested frequencies.

An explanation for the low loss tangent values in the Al:HfO_2 thin films could be due to a low concentration of defects. Many Hf-based thin films on initial application of electric field exhibit a pinched PE loop. However, upon further cycling the P_r increases, this phenomenon is known as the wake-up effect.[6,10,36,39,40] Lomenzo et al. and Zhou et al. both attributed the wake-up effect in Si:HfO_2 to the movement oxygen vacancies, which are believed to act as pinning sites for domain wall motion.[6,10] Furthermore, these vacancies were thought to have been induced by the oxidation of the TiN bottom electrode during growth.[6,10] Zhang et al. showed Al:HfO_2 thin films with TiN electrodes also experience wake-up and an irradiated set of films experienced an even faster wake up due to radiation induced defects, predominantly oxygen vacancies.[41] The effect electrodes have on oxygen vacancy concentration in undoped HfO_2 has also been explored, with Pt electrodes showing to induce less than TiN.[42] This is due to Pt having a lower oxygen affinity than TiN. The bottom electrodes for the samples in this work were Pt. The P_r values not showing increases over 1 μC/cm^2 for up to 10^4 cycles give credence to a lower oxygen vacancy concentration, resulting in the low loss tangent values. Another parameter shown to depend on defect concentration is leakage current.[43,44] The leakage current of our thin films being measured to be < 10 uA/cm^2 up to 3 MV/cm for each composition, again suggests a low defect concentration in the Al:HfO_2 thin films.

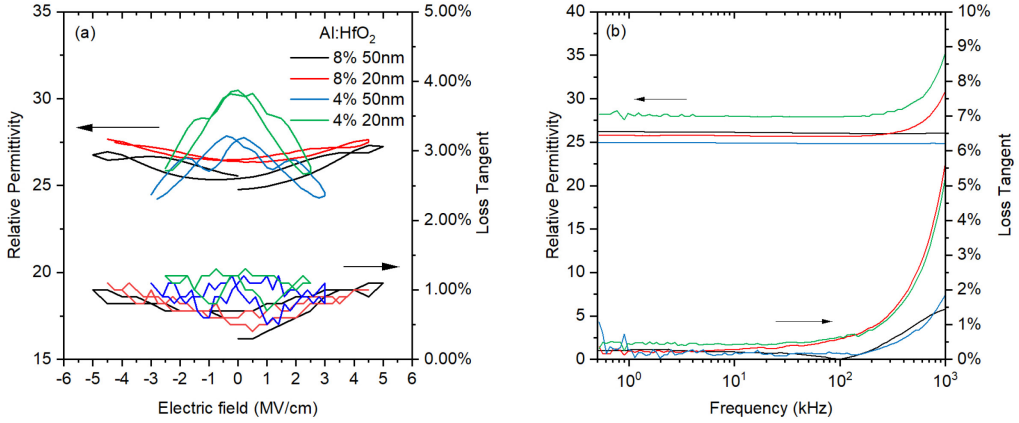

Figure 5: The dielectric constant and loss tangent vs. electric field (a) and frequency(b) for the Al:HfO_2 thin films.

In conclusion, Al-doped HfO_2 thin films of varying dopant concentration (4 at% or 8 at%) and varying thickness (20nm or 50nm) were studied using an energy storage application driven methodology. The PE loops of the Al:HfO_2 thin films revealed the 8 at% Al-doped samples had slimmer loops than that of the 4 at% Al:HfO_2 thin films. Thus, the 8 at% Al:HfO_2 samples had higher η values at equal applied fields than the 4 at% Al:HfO_2 samples. The 8 at% Al:HfO_2 samples could also withstand higher fields resulting in a maximum value of 63 J/cm^3 with an efficiency of 85% for the 50nm sample. As much as ESD values are reported, this study shows that considerations must be made not only to ESD, but also to E_{BD} and equally to V_{op}. In considering the eventual commercial use of these devices, the 8 at% Al:HfO_2 50nm sample showed the most promise with its ability withstand higher voltages and thus have higher ESD (2.865 J/cm^3) and η (100%) at V_{op} (8 V). The loss tangent values of our Al-doped HfO_2 thin films were the lowest recorded to date for HfO_2-based thin films at under 2%. The loss tangent also remained below 2% over a frequency range of 4 orders of magnitude (100Hz to 100kHz). The reliability study of the E_{BD} of the samples showed the 4 at% Al:HfO_2 thin film's E_{BD} was more consistent from device to device than the 8 at% Al:HfO_2 thin films. However, the 8 at% Al:HfO_2 still had narrow spreads of E_{BD} as indicated by $\beta \geq 6$. A holistic consideration of energy storage density and efficiency, combined with rarely measured loss tangent values provide guidance for materials in energy storage applications, highlighting the potential of high at% Al:HfO_2.

Supplementary Material

See supplementary material for the monopolar polarization vs. electric field loops of each sample that were used for the calculation of ESD values.

Acknowledgements

This project was supported in part by a fellowship at the US CCDC Army Research Laboratory, administered by Oak Ridge Associated Universities (ORAU) through the U.S. Department of Energy Oak Ridge Institute for Science and Education. AP and JJ acknowledge partial support from the National Science Foundation under award umber CMMI-1634955.

Data Availability

The data that supports the findings of this study are available from the corresponding author upon reasonable request.

References

[1] S. Kundu, D. Maurya, M. Clavel, Y. Zhou, N.N. Halder, M.K. Hudait, P. Banerji, and S. Priya, Scientific Reports **5**, 8494 (2015).
[2] J. Muller, P. Polakowski, S. Riedel, S. Mueller, E. Yurchuk, and T. Mikolajick, 2014 14th Annual Non-Volatile Memory Technology Symposium (NVMTS) (2014).
[3] T.F. Zhang, X.G. Tang, Q.X. Liu, Y.P. Jiang, L.L. Jiang, and L. Luo, Materials & Design **90**, 410 (2016).
[4] H. Cai, S. Yan, M. Zhou, N. Liu, J. Ye, S. Li, F. Cao, X. Dong, and G. Wang, Journal of the European Ceramic Society **39**, 4761 (2019).
[5] M.D. Nguyen and G. Rijnders, Journal of the European Ceramic Society **38**, 4953 (2018).
[6] P.D. Lomenzo, Q. Takmeel, C. Zhou, C.M. Fancher, E. Lambers, N.G. Rudawski, J.L. Jones, S. Moghaddam, and T. Nishida, Journal of Applied Physics **117**, 134105 (2015).
[7] R. Materlik, C. Künneth, and A. Kersch, Journal of Applied Physics **117**, 134109 (2015).
[8] X. Sang, E.D. Grimley, T. Schenk, U. Schroeder, and J.M. LeBeau, Appl. Phys. Lett. **106**, 162905 (2015).
[9] F. Huang, X. Chen, X. Liang, J. Qin, Y. Zhang, T. Huang, Z. Wang, B. Peng, P. Zhou, H. Lu, L. Zhang, L. Deng, M. Liu, Q. Liu, H. Tian, and L. Bi, Phys. Chem. Chem. Phys. **19**, 3486 (2017).
[10] D. Zhou, J. Xu, Q. Li, Y. Guan, F. Cao, X. Dong, J. Müller, T. Schenk, and U. Schröder, Appl. Phys. Lett. **103**, 192904 (2013).
[11] S.V. Barabash, J Comput Electron **16**, 1227 (2017).
[12] I. Burn and D.M. Smyth, Journal of Materials Science **7**, 339 (1972).
[13] X. Hao, J. Zhai, L.B. Kong, and Z. Xu, Progress in Materials Science **63**, 1 (2014).
[14] A.P. Sharma, D.K. Pradhan, S.K. Pradhan, and M. Bahoura, Scientific Reports **9**, 16809 (2019).
[15] P. Chen, S. Wu, P. Li, J. Zhai, and B. Shen, Inorg. Chem. Front. **5**, 2300 (2018).
[16] J. Kim, S. Saremi, M. Acharya, G. Velarde, E. Parsonnet, P. Donahue, A. Qualls, D. Garcia, and L.W. Martin, Science **369**, 81 (2020).
[17] F. Ali, X. Liu, D. Zhou, X. Yang, J. Xu, T. Schenk, J. Müller, U. Schroeder, F. Cao, and X. Dong, Journal of Applied Physics **122**, 144105 (2017).
[18] M.H. Park, H.J. Kim, Y.J. Kim, T. Moon, K.D. Kim, and C.S. Hwang, Advanced Energy Materials **4**, 1400610 (2014).
[19] P.D. Lomenzo, C.-C. Chung, C. Zhou, J.L. Jones, and T. Nishida, Appl. Phys. Lett. **110**, 232904 (2017).
[20] X.J. Lou, Appl. Phys. Lett. **94**, 072901 (2009).
[21] L. Zhou, R.Z. Zuo, G. Rixecker, A. Zimmermann, T. Utschig, and F. Aldinger, Journal of Applied Physics **99**, 044102 (2006).
[22] B. Chu, Y. Zhou, and S. Zhang, in *Dielectric Polymer Materials for High-Density Energy Storage*, edited by Z.-M. Dang (William Andrew Publishing, 2018), pp. 351–382.
[23] Q.Y. Jiang, E.C. Subbarao, and L.E. Cross, Journal of Applied Physics **75**, 7433 (1994).
[24] J.H. Jang, K.H. Yoon, and H.J. Shin, Appl. Phys. Lett. **73**, 1823 (1998).
[25] X. Liu, D. Zhou, Y. Guan, S. Li, F. Cao, and X. Dong, Acta Materialia **154**, 190 (2018).
[26] C. Sire, S. Blonkowski, M.J. Gordon, and T. Baron, Appl. Phys. Lett. **91**, 242905 (2007).
[27] B. Hanrahan, C. Mart, T. Kämpfe, M. Czernohorsky, W. Weinreich, and A. Smith, Energy Technology **7**, 1900515 (2019).
[28] P. Jain and E.J. Rymaszewski, IEEE Transactions on Advanced Packaging **25**, 454 (2002).
[29] J. Pérez de la Cruz, E. Joanni, P.M. Vilarinho, and A.L. Kholkin, Journal of Applied Physics **108**, 114106 (2010).
[30] F. He, W. Ren, G. Liang, P. Shi, X. Wu, and X. Chen, Ceramics International **39**, S481 (2013).
[31] J. Liang, P. Li, D. Wang, X. Fang, J. Ding, J. Wu, and C. Tang, Materials (Basel) **9**, (2016).
[32] S. Jachalke, T. Schenk, M.H. Park, U. Schroeder, T. Mikolajick, H. Stöcker, E. Mehner, and D.C. Meyer, Appl. Phys. Lett. **112**, 142901 (2018).
[33] H. Domingos, D. Quattro, and J. Scaturro, IEEE Transactions on Components, Hybrids, and Manufacturing Technology **1**, 423 (1978).

[34] B. Long, M. Prevallet, J.D. Prymak, and E. Woodfield, in *CARTS* (Palm Springs, CA, 2005), p. 5.
[35] J. Müller, S. Knebel, D. Bräuhaus, and U. Schröder, Appl. Phys. Lett. **100**, 082905 (2012).
[36] E.D. Grimley, T. Schenk, X. Sang, M. Pešić, U. Schroeder, T. Mikolajick, and J.M. LeBeau, Advanced Electronic Materials **2**, 1600173 (2016).
[37] K. Kühnel, M. Czernohorsky, C. Mart, and W. Weinreich, Journal of Vacuum Science & Technology B **37**, 021401 (2019).
[38] J.D. Sullivan and P.H. Lauzon, J Mater Sci Lett **5**, 1245 (1986).
[39] U. Schröder, E. Yurchuk, J. Müller, D. Martin, T. Schenk, P. Polakowski, C. Adelmann, M.I. Popovici, S.V. Kalinin, and T. Mikolajick, Jpn. J. Appl. Phys. **53**, (2014).
[40] T.Y. Lee, K. Lee, H.H. Lim, M.S. Song, S.M. Yang, H.K. Yoo, D.I. Suh, Z. Zhu, A. Yoon, M.R. MacDonald, X. Lei, H.Y. Jeong, D. Lee, K. Park, J. Park, and S.C. Chae, ACS Appl. Mater. Interfaces **11**, 3142 (2019).
[41] W.L. Zhang, Y.H. Mao, L. Cui, M.H. Tang, P.Y. Su, X.J. Long, Y.G. Xiao, and S.A. Yan, Phys. Chem. Chem. Phys. **22**, 21893 (2020).
[42] W. Zhang, J.-Z. Kong, Z.-Y. Cao, A.-D. Li, L.-G. Wang, L. Zhu, X. Li, Y.-Q. Cao, and D. Wu, Nanoscale Res Lett **12**, 393 (2017).
[43] X. Tang, L. Jin, J. Dai, X. Zhu, and Y. Sun, Journal of Alloys and Compounds **695**, 2458 (2017).
[44] K.-H. Cho, C.-H. Choi, J.-Y. Choi, T.-G. Seong, S. Nahm, C.-Y. Kang, S.-J. Yoon, and J.-H. Kim, Journal of the European Ceramic Society **30**, 513 (2010).